11-1996

Characterization of Sr-Doped $LaMnO_3$ and $LaCoO_3$ as Cathode Materials for a Doped $LaGaO_3$ Ceramic Fuel Cell

Kevin Huang
University of South Carolina - Columbia, huang46@cec.sc.edu

Man Feng

John B. Goodenough

Michael Schmerling

Publication Info

Published in *Journal of The Electrochemical Society*, Volume 143, Issue 11, 1996, pages 3630-3636.

Publisher's Version: http://dx.doi.org/10.1149/1.1837262
Huang, K., Feng, M., Goodenough, J. B., & Schmerling, M. (1996). Characterization of Sr-Doped $LaMnO_3$ and $LaCoO_3$ as Cathode Materials for a Doped $LaGaO_3$ Ceramic Fuel Cell. Journal of The Electrochemical Society, 143 (11), 3630-3636. http://dx.doi.org/10.1149/1.1837262

Characterization of Sr-Doped $LaMnO_3$ and $LaCoO_3$ as Cathode Materials for a Doped $LaGaO_3$ Ceramic Fuel Cell

Keqin Huang,* Man Feng,* John B. Goodenough, and Michael Schmerling

Center for Material Science and Engineering, The University of Texas at Austin, Austin, Texas 78712, USA

ABSTRACT

Energy dispersive spectrometry line scan and ac impedance spectroscopy were used in this study to investigate the chemical reactions between two cathode materials, $La_{0.84}Sr_{0.16}MnO_3$ (LSM), $La_{0.5}Sr_{0.5}CoO_{3-\delta}$ (LSC), and the electrolyte $La_{0.9}Sr_{0.1}Ga_{0.8}Mg_{0.2}O_{2.85}$ (LSGM). Significant interdiffusions of Co into LSGM and Ga into LSC were found at an LSC/LSGM interface even at relatively low fabrication temperatures. In contrast, only small interdiffusions of Mn into LSGM and Ga into LSM were detected at the LSM/LSGM interface even though it was fired at 1470°C. The ac impedance spectra of the electrolyte LSGM with LSM, LSC, and Pt electrodes indicate a grain-boundary contribution to the total conductivity in the intermediate frequency range and a diffusion-controlled impedance in the low-frequency range. Irrespective of chemical reactions and a larger thermal expansion coefficient, LSC has the lowest dc resistance of all three electrodes investigated. Considering both the small interdiffusion reactions between LSM and LSGM and their similar thermal expansion coefficients, LSM could be an appropriate cathode material for LSGM-based fuel cells.

Introduction

The doped lanthanum gallate perovskite, $La_{0.9}Sr_{0.1}Ga_{0.8}Mg_{0.2}O_{2.85}$ (LSGM), has been found to be an excellent oxide-ion conductor over a broad range of oxygen partial pressures[1-3] with a typical conductivity $\sigma_O \geq 0.10$ S/cm at 800°C. Thus it becomes a strong candidate for the electrolyte replacing the current Y_2O_3- stabilized ZrO_2 in a solid oxide fuel cell (SOFC) operating around 800°C. Appropriate cathode and anode materials compatible with this electrolyte are also critical to the success of such a ceramic fuel cell.

A cathode material must not only be chemically, morphologically, and dimensionally stable; it must also possess high electronic conductivity to support electron flow in the oxidizing environment. The cathode must perform three functions: chemisorb dioxygen, reduce the chemisorbed dioxygen to two oxide ions, and deliver the oxide ions to the electrolyte. If the cathode is not an oxide-ion conductor, the reduction must take place at a three-phase interface of gaseous O_2, electrode, and electrolyte. In order to obtain a sufficient three-phase area, relatively thick and porous electrode/electrolyte composite films must be employed, which create an additional tortuous pathway that the oxide ions must travel over. If the cathode is a mixed electronic/oxide-ion conductor on which dioxygen chemisorbs, then only a thin-film electrode is needed provided good oxide-ion transfer occurs across the electrolyte/electrode interface. In this case, dioxygen is reduced on one side of the electrode film, and it is delivered to the electrolyte on the opposite side. The second solution to the electrode problem is clearly preferable to the first provided a suitable mixed electron/oxide-ion conductor can be identified.

The perovskite $LaSrCo_3O_{3-\delta}$ (LSC) has been identified as a good mixed electron/oxide-ion conductor; it retains its oxygen-deficiency even in an oxidizing atmosphere.[4-11] However, due to a low-spin to high-spin transition at the Co(III) ions, it has a significantly higher thermal expansion coefficient than Y_2O_3-stabilized ZrO_2[12] and it reacts chemically with the electrolyte to form a blocking layer of the pyrochlore $La_2Zr_2O_7$ at the interface.[13,14] Therefore it is unsuitable for use with the stabilized-ZrO_2 electrolytes.

The alternative cathode material that has been extensively studied is $La_{0.84}Sr_{0.16}MnO_3$ (LSM), which exhibits metallic conduction in an oxidizing atmosphere in the operating temperature range of an SOFC. It also has a thermal expansion that approaches that of Y_2O_3-stabilized ZrO_2, but it is not an oxide-ion conductor. In an oxidizing atmosphere, the oxygen sites are fully occupied; there can be no interstitial oxygen. Nevertheless, LSM has been extensively applied as a porous composite cathode even though it, too, reacts with stabilized ZrO_2 at higher operating temperatures to form a blocking $La_2Zr_2O_7$ layer at the electrode/electrolyte interface.[15-19] With higher Sr doping, the perovskite $SrZrO_3$ may also form at the electrode/electrolyte interface with both LSC and LSM.[20,21] These chemical reactions occur during both fabrication of a cell and at the higher operating temperatures required with stabilized-ZrO_2 electrolytes; they have plagued the development of a satisfactory cathode for an SOFC using a stabilized-ZrO_2 electrolyte.

In this paper we investigate whether chemical reactions also occur between the electrolyte LSGM and either of these electrode materials. Since the two cathode materials have the same perovskite structure as LSGM, interdiffusion of elements across an interface can be anticipated. An energy dispersive spectroscopy (EDS) technique has been used to monitor interdiffusion of the elements across the cathode/electrolyte interface. The thermal expansion coefficient of LSGM and the impedance spectra of LSGM with LSM and LSC as electrode materials have also been measured. The possible use of LSM and LSC as cathode materials in LSGM-based fuel cells has been evaluated.

Experimental

The electrolyte $La_{0.9}Sr_{0.1}Ga_{0.8}Mg_{0.2}O_{2.85}$ was made by solid-state reaction as described in Ref. 2. Stoichiometric

* Electrochemical Society Student Member.

amounts of La_2O_3, $SrCO_3$, Ga_2O_3, and MgO were mixed with the aid of acetone and fired at 1250°C overnight. After regrinding and pelletizing, the mixture was finally sintered at 1470°C for 36 h. Similarly, $SrCO_3$, La_2O_3, MnO_2, and Co_3O_4 were used to make $La_{0.84}Sr_{0.16}MnO_3$ and $La_{0.5}Sr_{0.5}CoO_{3-\delta}$; sinterings were performed at 1400 and 1250°C, respectively. All materials were examined by powder x-ray diffraction.

To prepare a suitable cathode/electrolyte interface for study, powders of cathode LSM and electrolyte LSGM were first micronized separately in a milling machine with corundum balls and cold-pressed into separate small pellets; the two pellets were then pressed together and sintered in ambient atmosphere at 1470°C for 36 h in order to maximize any chemical reaction between them and form a good bond. In the case of LSC, an LSC slurry was coated on the surface of LSGM pellets and sintered at 1050°C for 2 h.

To investigate the extent of the interdiffusion elements across the interfaces during their formation under these heat-treatments, we did an EDS analysis in the line-scan mode. For these experiments, the compound pellets were sectioned perpendicularly and carbon-coated before being scanned by the electron microscope. A 25 keV electron beam was incident vertically onto the surface, and the x-ray emergence angle for the detection was 35°. The x-ray energies chosen for analysis were K_α = 9.25 keV for Ga, K_α = 5.90 keV for Mn, K_α = 6.93 keV for Co, L_α = 4.65 keV for La, K_α = 1.25 keV for Mg, and L_α = 1.69 keV for Sr. The manganese and cobalt contents were standardized with spectrum-pure manganese and Co_3O_4 powders, respectively.

In order to test further for a possible chemical interaction between the LSM and LSGM materials, we performed a second experiment. Equal weights of LSGM and LSM powders were mixed, ground, formed into pellets, and sintered at 1470°C for 10 h. X-ray diffraction was performed on pulverized powders before and after sintering to see whether there was any change in the powder diffraction patterns.

The same preparation routine for the two cathode materials was used as electrodes in our ac impedance spectroscopy measurements. Powders of LSM and LSC were dispersed in an organic binder (from Heraeus) and pasted onto both surfaces of an LSGM pellet. The pellets were baked at 1050°C for 2 h before being loaded into a measuring furnace and heated to 800°C. For comparisons Pt electrodes prepared from platinum paste (from Heraeus) were also fabricated. The impedance spectra of LSGM cells with all three electrodes were measured with an HP 4192A LF impedance analyzer from 800 to 320°C in air. The bulk and total conductivities of LSGM were extracted from the intersections with the real-axis of related bulk and grain-boundary semicircles in the impedance spectra. The thermal expansion coefficient of an LSGM pellet was measured with a Perkin-Elmer TMA7 thermal analyzer from room temperature to 850°C.

Results

Powder x-ray diffraction.—The powder x-ray diffraction pattern of $La_{0.9}Sr_{0.1}Ga_{0.8}Mg_{0.2}O_{2.85}$ (LSGM) can be indexed into a primitive cubic crystal structure with a lattice parameter a = 3.911(3) Å.[1-3] A small amount of $LaSrGaO_4$ impurity is detected in the patterns. The patterns of $La_{0.84}Sr_{0.16}MnO_3$ (LSM) and $La_{0.5}Sr_{0.5}CoO_{3-\delta}$ (LSC) show a single monoclinic and primitive cubic phase, respectively. Although the main peaks of the powder x-ray diffraction patterns of LSGM and LSM overlap, as shown in Fig. 1, no new phase is formed and little change occurs in the pattern even after sintering the intimately mixed fine powders of LSGM and LSM at 1470°C for 10 h.

SEM/EDS analysis.—The interface of LSM/LSGM under SEM observation is shown in Fig. 2a. We collected an EDS spectrum across the LSGM/LSM interface from LSM to LSGM in 30 steps over 100 μm (determined from the CRT display). Figure 2b shows three distinguishable regions. Region (I) has constant La, Sr, and Mn contents

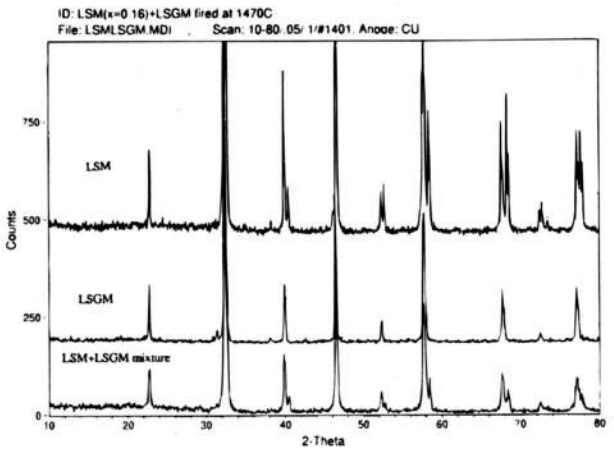

Fig. 1. X-ray diffraction patterns of LSM, LSGM, and equal weight mixtures of LSM and LSGM after sintering at 1470°C for 10 h.

corresponding to bulk LSM. The gallium content increases while the manganese content decreases within a range of 20 μm in a narrow interdiffusion region (II). In region (III), the La, Sr, and Ga contents return to a constant value corresponding to bulk LSGM. The residual amount of Mn (~1%) at the LSGM side of the sample is due to the overlapping of La L_α lines with the Mn K_α line; it is not a meas-

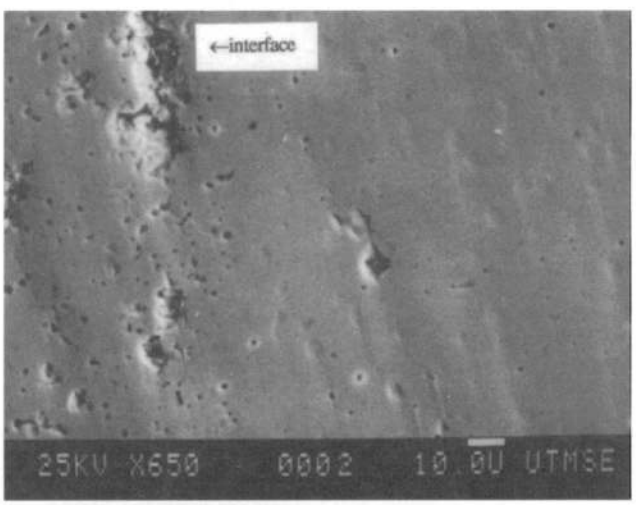

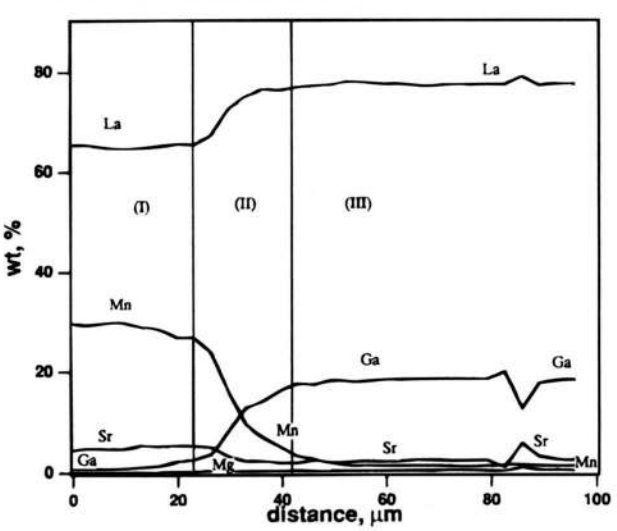

Fig. 2. The LSM/LSGM interface: (a, top) SEM and (b, bottom) EDS analysis of element distribution.

ure of Mn concentration. The EDS spectrum in region (III) is essentially the same as that from a pure LSGM pellet. The one fluctuation of La, Ga, and Sr contents in region (III) indicates a grain boundary (impurity $LaSrGaO_4$) was detected.

These results show that no significant interdiffusion of Mn into LSGM and Ga into LSM occurs at 1470°C even with internally mixed fine powder. A manufacturer can co-fire the cathode and the electrolyte in a single step.

Figure 3a shows the fracture of LSC/LSGM under the SEM. The line scan was started inside LSGM about 80 μm away from the LSC/LSGM interface. The EDS spectrum, as shown in Fig. 3b, can also be divided into three parts. Region (I) extends from well inside the bulk LSGM to about 25 μm from the interface, region (II) extends to the interface, and region (III) is on the LSC side of the interface. Region (I) contains constant La, Sr, Mg, and Ga contents and no Co; region (II) shows a strong cobalt content with a sharp interdiffusion front at the boundary between region (I) and (II) and a depletion of Ga from the interface. Region (III) shows a continuous increase of Co and a sharp interdiffusion front of Ga into LSC at about 20 μm from the interface. Our measurements stop at what would appear to be the edge of a bulk LSC region (III). These results show that a significant interdiffusion of Co into LSGM and Ga into LSC occurred during the interface fabrication at 1050°C for 2 h. The fluctuation of La, Sr, and Ga contents in region (II) is associated with a grain boundary.

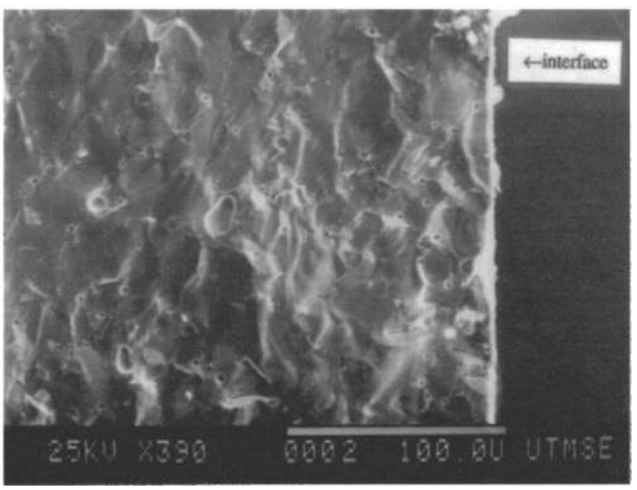

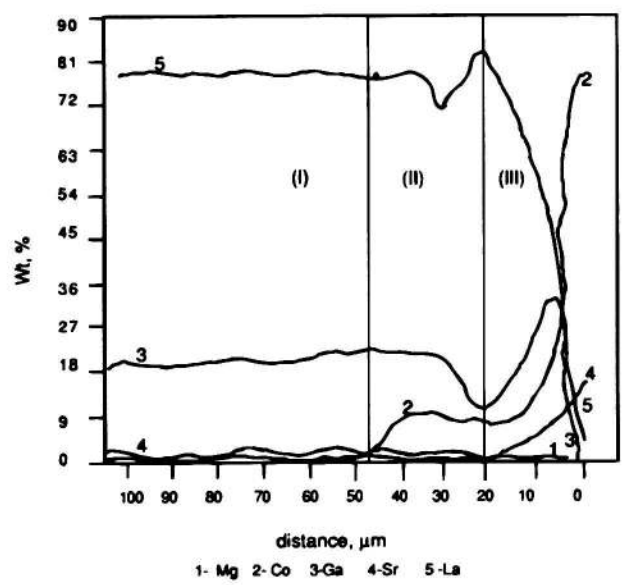

Fig. 3. The LSC/LSGM interface: (a, top) SEM and (b, bottom) EDS analysis of element distribution.

Impedance spectroscopy.—With all three-electrode materials (LSM, LSC, and Pt), the impedance spectra for the LSGM pellets could be resolved into a bulk (grain) semicircle, a grain boundary semicircle, and an electrode process arc. Typical spectra and their related equivalent circuits are shown in Fig. 4.

Bulk (grain) semicircle.—With all three electrodes, the bulk (grain) semicircle was perfect; it corresponds to a parallel R_b and C_b circuit. With R_b obtained from the intersection of this semicircle with the real-axis, C_b can be calculated from $\omega_p R_b C_b = 1$, where ω_p is the peak frequency of the bulk semicircle. The C_b values calculated over the temperature 320 to 441°C, Table I, are insensitive to both the temperature and the type of electrode used. For temperatures $T > 441$°C, the dielectric relaxation time $\tau = R_b C_b$ becomes too small ($<10^{-7}$ s) for ω_p to fall in the frequency range of our measurement.

Grain-boundary semicircle.—As shown in Fig. 9, the activation energies for the bulk and total conductivities are equal within a certain temperature range (<600°C). Where this occurs, good intergranular contact appears to be made across regions of the grain boundaries. Therefore, following Bauerle,[19] we introduce a parallel resistance R_c for the intergranular "easy ionic pathway" in our equivalent circuit for the grain boundaries. Since the permittivity of the grain boundary is similar to that of the bulk ($\varepsilon_b \approx \varepsilon_{gb}$), the introduction of an R_c should not change C_{gb} significantly. Observations of a polished LSGM after thermal etching, Fig. 5, reveal preferential segregation of the plate-like second-phase $LaSrGaO_4$ to the grain boundaries; the small contact regions between the second-phase particles represent the areas of good intergranular contact.

The fraction of ionic current that is blocked by the grain boundaries is given by the blocking coefficient[20]

$$\beta = R_{gb}/R_{total} = R_{gb}/(R_{gb} + R_b) \quad [1]$$

The temperature dependence of β, Fig. 6, shows a rapid decrease in the range $600 < T < 800$°C. It appears that the second phase precipitated in the grain boundaries either dissolves or becomes more conductive.

Electrode process arc.—The low-frequency arc reflects processes occurring at the electrode/electrolyte interfaces. For the LSM electrode, the impedance spectrum shows a typical Warburg semi-infinite diffusion impedance in the low-frequency range. The intersection angle of this part of the impedance with the real-axis remains constant at 45°. This Warburg impedance Z_w is given by[21]

$$Z_w = \frac{RT}{n^2F^2c_O\sqrt{2\omega D_O}}(1-j) \quad [2]$$

where $n = 2$ is the number of electrons transferred in the reaction $(1/2)O_2 + 2e^- = O^{2-}$, c_O is the surface concentration of oxygen atoms, D_O is the diffusion coefficient of oxygen atom at the surface, ω is the angular frequency, and R, T, and F have their usual meanings. Figure 7 shows the linear relationship at different temperatures between the real-part Z' of Z_w and $\omega^{-1/2}$ as given in Eq. 2; $c_O D_O^{1/2}$ can be calculated from the slope of each line. The plot of log $(c_O D_O^{1/2})$ *vs.* $1/T$ is a straight line, shown in Fig. 8; it gives a motional activation energy $\Delta H_m = 0.54$ eV for oxygen diffusion if we assume c_O is independent of the temperature. This value of ΔH_m is similar to that obtained for oxygen-vacancy migration in some oxide-ion conductors.

The impedance spectrum with Pt electrodes also shows an intersection angle of 45° with the real-axis for the electrode process arc; however, a curvature appears at very low frequency, especially at higher temperatures. Because of the porous microstructure of Pt electrodes prepared from pyrolysis of Pt paste, it is well accepted that the diffusion of oxygen atoms in a Pt electrode proceeds for a finite length along the LSGM-Pt-gas three-phase inter-

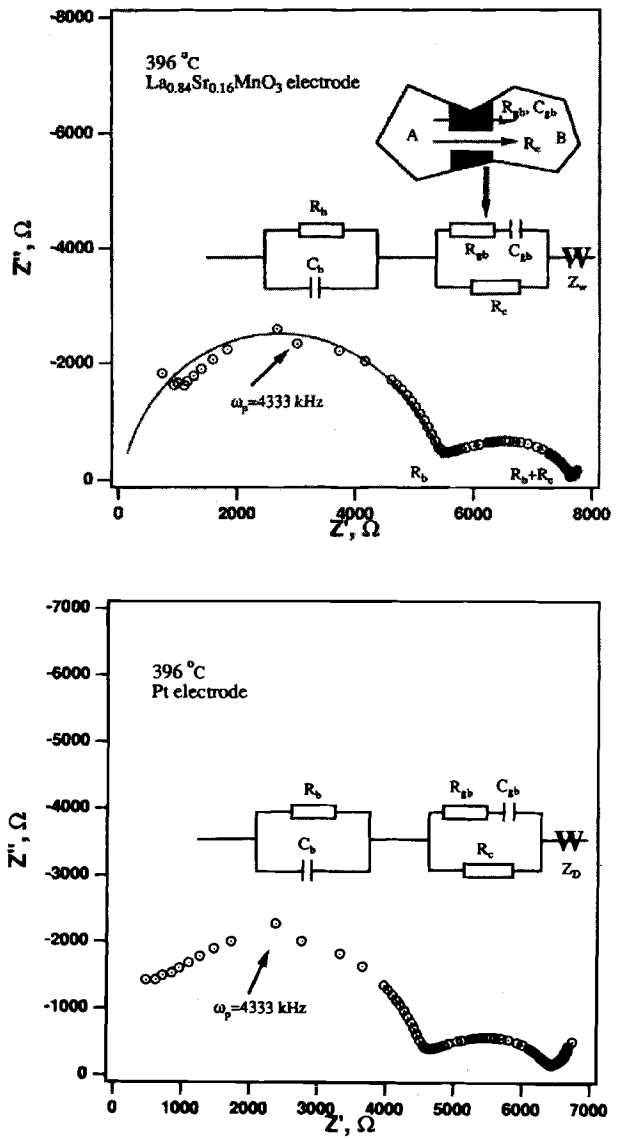

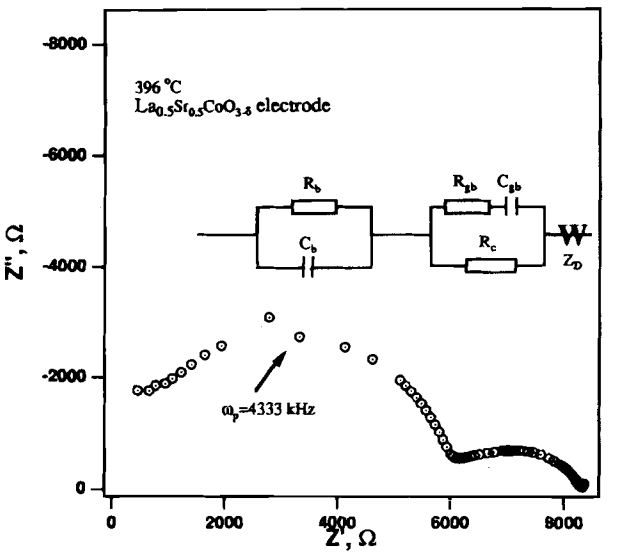

Fig. 4. AC impedance spectroscopy of LSGM at 396°C and equivalent circuits for three kinds of electrodes: (a, top left) LSM, (b, above) LSC, (c, left) Pt.

face before electrode reaction occurs. With this model, the diffusion impedance Z_D is given by[21]

$$Z_D = \frac{RT}{n^2F^2c_O}\frac{\tanh\delta\sqrt{(j\omega/D_O)}}{\sqrt{(j\omega D_O)}} \quad [3]$$

where δ is the diffusion distance of the oxygen atom along the interface and the other terms have the same meaning as in Eq. 2. The determination of D_O needs an even lower frequency range than is available in our experimental setup.

The intersection angles of the low-frequency electrode-process arc in the LSC impedance spectra are greater than 45°; they approach 90° at lower temperatures, which implies that a low dc resistance exists in the LSC electrode. This low electrode resistance may be attributed to a high conductivity for both electrons and oxide ions, which increases the electrode reaction area. Table II lists the coefficient α for three electrodes at several temperatures, where α is defined as $(R_{5Hz} - R_{total})/R_{5Hz}$ and represents the fraction of the total impedance that is due to the electrode impedance. From this table we can conclude that LSC possesses the best electrochemical performance of the three electrodes investigated irrespective of its chemical reactions with LSGM and larger thermal expansion coefficient than LSGM.

Arrhenius plot.—Figure 9 represents the Arrhenius plot for the bulk and total conductivities of LSGM obtained with the three electrodes investigated in this study. The activation energies for oxide-ion motion in the grain and grain-boundary regions are identical below 600°C for all three electrodes. This observation led to the easy path model in the section on Grain boundary semicircle. The

Table I. Comparisons of grain capacitance of LSGM using three kinds of electrodes.

Electrodes	T (°C)	320	331	344	356	369	381	396	410	425	441
LSM	C_b, pF	7.0	7.0	6.9	7.5	7.4	8.5	6.7	7.8	7.3	7.0
LSC	C_b, pF	9.2	8.3	7.6	7.9	7.0	7.8	6.1	6.9	6.3	5.9
Pt	C_b, pF	8.2	7.1	7.3	8.2	6.9	7.1	8.0	7.9	7.1	8.5

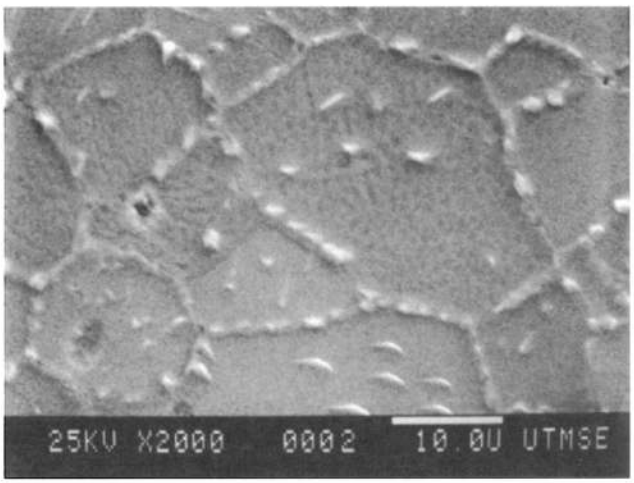

Fig. 5. Microstructure of LSGM under the SEM after thermal etching at 1350°C for 2 h.

convergence of the bulk and total conductivities above 600°C implies the second phase at the grain boundary either becomes more conductive or is dissolved.

In principle the bulk and grain-boundary properties have nothing to do with the choice of electrodes. However, the difference in the bulk conductivities measured with different electrodes indicates lower oxide-ion conductivity across the LSC/LSGM and LSM/LSGM interfaces. The poorer bonding of LSC and LSM to LSGM than obtained with Pt may be the reason for the difference in conductivities measured. The EDS analysis has revealed a remarkable interdiffusion of Co into LSGM and Ga into LSC. This interdiffusion may be deleterious to cell performance.

The curvature in the Arrhenius plot of Fig. 9 has been discussed in Ref. 22; we believe it comes from a short-range order-disorder transition. Whether it is related to a dissolution of the $LaSrGaO_4$ second phase from the grain boundaries remains unresolved.

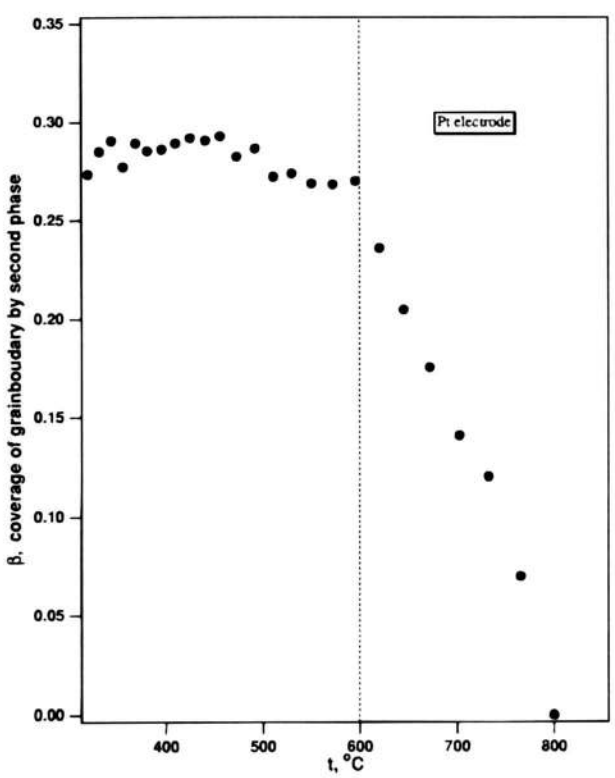

Fig. 6. The temperature dependence of the grain-boundary coverage by a second phase as measured with Pt electrodes.

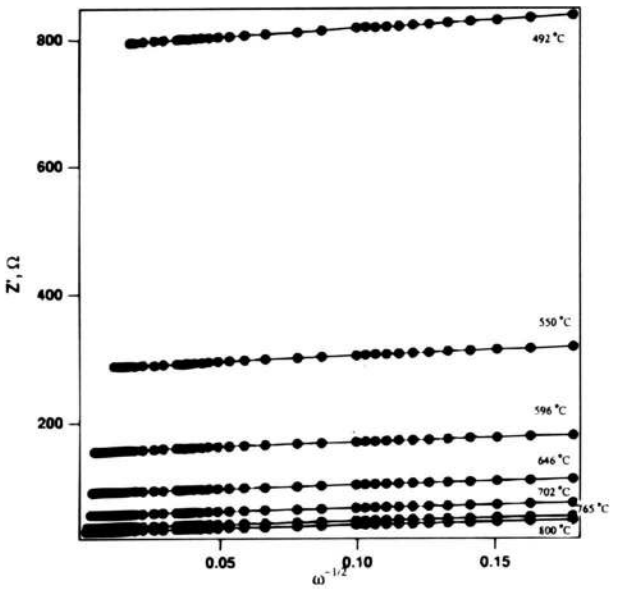

Fig. 7. The angular fequency dependence of the real-part of the impedance as obtained with LSM electrodes.

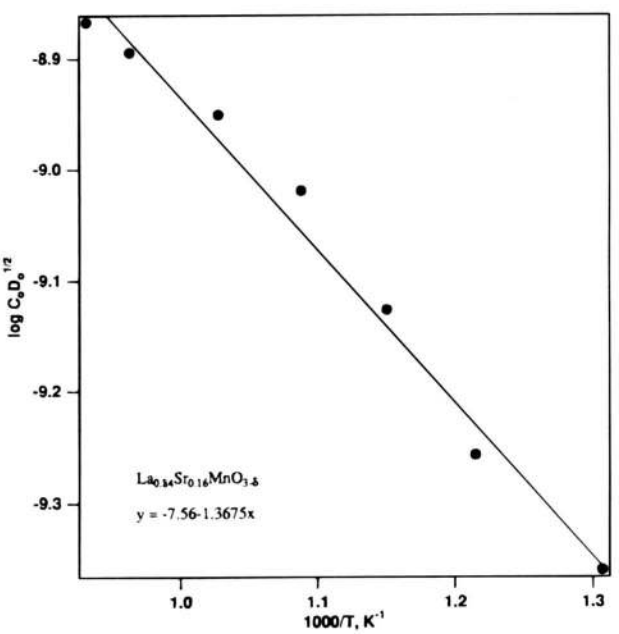

Fig. 8. The linear relationship between log ($c_O D_O^{1/2}$) and $1/T$.

Conclusions

A significant interdiffusion of Co into LSGM and Ga into LSC occurs at the LSC/LSGM interface, as determined

Table II. Comparison of α with three electrodes at several temperatures

α (%) Electrodes	T	800°C	702°C	596°C	492°C	396°C
LSM		72.2	64.7	53.6	35.4	4.79
LSC		23.1	18.2	5.80	1.34	0.574
Pt		69.4	67.7	50.5	21.0	4.73

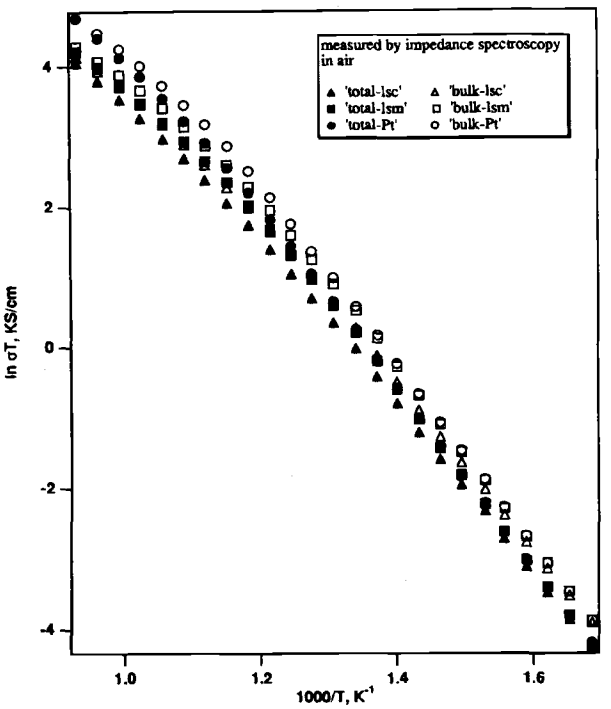

Fig. 9. Arrhenius plot of bulk and total conductivities obtained with the three different electrodes.

with the EDS line-scan technique, even though the interface was fired at 1050°C for only 2 h. Nevertheless in the thick sample used, the LSC gave the lowest dc electrode resistance. The high thermal-expansion coefficient relative to that of LSGM may induce the interdiffusion and prevent LSC from being an appropriate cathode for LSGM. The relatively small interdiffusion across the LSM/LSGM interface, even after firing at 1470°C for 36 h, and a similar thermal expansion coefficient compared to LSGM makes LSM a viable cathode candidate for an LSGM-based ceramic fuel cell. However, search for another cathode material that posseses both high electronic and oxide-ion conduction and similar thermal expansion match to the electrolyte LSGM is still needed. Table III lists some typical technical data for LSGM, LSM, and LSC.

Acknowledgement

We would like to thank Electric Power Research Institute for financial support. Dr. Wate T. Bakker is the manager of this project.

Manuscript received June 19, 1996.

The University of Texas at Austin assisted in meeting the publication costs of this article.

REFERENCES

1. T. Ishihara, H. Matruda, and Y. Takita, *J. Am. Chem. Soc.*, **116**, 3801 (1994).
2. M. Feng and J. B. Goodenough, *Eur. J. Solid State Inorg. Chem.*, **31**, 663 (1994).
3. K. Huang, M. Feng, and J. B. Goodenough, *J. Am. Ceram. Soc.*, **79**, 1100 (1996).
4. J. Kjær, I. G. Krogh-Anderson, N. Mogensen *et al.* in *Proceedings of the 14th Risø International Symposium on Materials Science, High Temperature Electrochemical Behaviour of Fast Ion and Mixed Conductors*, F. W. Poulson, J. J. Bentzen, T. Jacobsen, E. Skou, and M. J. L. Østergård, Editors, Roskilde, Denmark (1993).
5. J. Mizusaki, Y. Mima, S. Yamauchi, and K. Fueki, *This Journal*, **136**, 2082 (1989).
6. A. N. Petrov and P. Kofstad, in *Proceedings of the 3rd International Symposium on Solid State Fuel Cells*, S. C. Singhal and H. Iwahara, Editors, PV 93-4, p. 220, The Electrochemical Society Proceedings Series, Pennington, NJ (1993).
7. Y. Ohno, S. Nagata, and H. Sato, *Solid State Ionics*, **9&10**, 1001 (1983).
8. Y. Ohno, S. Nagata, and H. Sato, *ibid.*, **3/4**, 439 (1981).
9. I. F. Kononyuk, S. P. Tolochko, V. A. Lutsko, and V. M. Anishchik, *J. Solid State Chem.*, **48**, 209 (1983).
10. J. Echigoya, H. Hiratsuka, and H. Sato, *Mater. Trans. JIM*, **30**, 789 (1989).
11. O. Yamamoto, Y. Takeda, R. Kanno, and T. Kojima, in *Proceedings of 1st International Symposium on Solid Oxide Fuel Cells*, S. C. Singhal, Editor, PV 89-11, p. 242, The Electrochemical Society Proceedings Series, Pennington, NJ (1989).
12. O. Yamamoto, Y. Takeda, and T. Kojima, in *Proceedings of International Symposium on Solid Oxide Fuel Cells*, O. Yamamoto, M. Dokiya, and H. Tagawa, Editors, Science House, Nagoya, Japan (1989).
13. C. C. Chen, M. M. Nashrallah, and H. U. Anderson, in *Proceedings of the 3rd International Symposium on Solid State Fuel Cells*, S. C. Singhal and H. Iwahara, Editors, PV 93-4, p. 252, The Electrochemical Society Proceedings Series, Pennington, NJ (1993).
14. H. Tagawa, J. Mizusaki, M. Katou, K. Hirano, A. Sawata, and K. Tsuneyoshi, in *Proceedings of the 2nd International Symposium on Solid State Fuel Cells*, F. Grosz, P. Zegers, S. C. Singhal, and O. Yamamoto, Editors, Commission of the European Communities, Luxembourg (1991).
15. C. Milliken, D. Tucker, S. Elangovan, and A. Khandkar, in 1990 Fuel Cell Seminar Abstracts, Courtesy Associates, Washington, DC (1990).
16. H. Yokokawa, N. Sakai, T. Kawada, and M. Dokiya, *This Journal*, **138**, 2719 (1991).
17. H. Yokokawa, N. Sakai, T. Kawada, and M. Dokiya, in *Proceedings of the 2nd International Symposium on Solid State Fuel Cells*, F. Grosz, P. Zegers, S. C. Singhal, and O. Yamamoto, Editors, Commission of the European Communities, Luxembourg (1991).
18. J. A. M. van Roosmalen and E. H. P. Cordfunke, *Solid State Ionics*, **52**, 303 (1992).
19. J. E. Bauerle, *J. Phy. Chem. Solids*, **30**, 2657 (1969).
20. E. J. L. Schouler, G. Giroud, and M. Kleitz, *J. Chim. Phys.*, **70**, 1309 (1983).
21. D. Braunshtein, D. S. Tannhauser, and I. Reiss, *This*

Table III. Comparisons of technical data between LSGM, LSM, and LSC.

Compound properties	LSGM	LSM	LSC	Ref.
Composition	$La_{0.9}Sr_{0.1}Ga_{0.8}Mg_{0.2}O_{2.85}$	$La_{0.84}Sr_{0.16}MnO_3$	$La_{0.5}Sr_{0.5}CoO_{3-\delta}$	1, 4, 11
Typical conductivity	~0.10 S/cm at 800°C	~150 S/cm at 1000°C	~1000 S/cm at 1000°C	1, 24, 5
TEC[a]	12.47[b]	~12.0	~20.0	10, 23
$\times 10^{-6}$/K	(613 to 850°C)	(25 to 1000°C)	(25 to 1000°C)	
Chemical stability	$1 < P_{O_2} < 10^{-22}$ atm at 800°C	Decomposes at 1000°C if $P_{O_2} < 10^{-14}$ atm, Sr doping reduces stability	Decomposes at 1000°C if $P_{O_2} < 10^{-7}$ atm, Sr doping reduces stability	25, 26

[a] TEC denotes thermal expansion coefficient.
[b] This study.

Journal, **128**, 82 (1981).
22. K. Huang, M. Feng, and J. B. Goodenough, *J. Am. Chem. Soc.*, Submitted.
23. E. Ivers-Tiffé, M. Schießl, H. J. Oel, and W. Wersing, in *Proceedings of the 14th Risø International Symposium on Materials Science, High Temperature Electrochemical Behaviour of Fast Ion and Mixed Conductors*, F. W. Poulson, J. J. Bentzen, T. Jacobsen, E. Skou, and M. J. L. Østergård, Editors, Roskilde, Denmark (1993).
24. J. H. Kuo, H. U. Anderson, and D. M. Sparlin, *J. Solid State Chem.*, **87**, 55 (1990).
25. T. Nakamura, G. Petzow, and L. J. Gauckler, *Mater. Res. Bull.*, **14**, 649 (1979).
26. O. M. Sreedharan, P. Pankajavalli, and J. B. Gnanamoorthy, *High Temp. Sci.*, **16**, 251 (1983).

Inductive Loops in Impedance Spectroscopy Caused by Electrical Shielding

J. Fleig, J. Jamnik,[a] and J. Maier

Max-Planck-Institut für Festkörperforschung, 70569 Stuttgart, Germany

J. Ludvig*

Lehrstuhl für Informatik V, Universität Mannheim, 68131 Mannheim, Germany

ABSTRACT

The electrical shielding of the sample which is inevitable for the measurement of high impedances can lead to significant anomalies in the measured impedance. The displacement current, which flows between the sample and the shield, can result in "inductive loops" appearing in the impedance spectra at low frequencies. Experimental results are presented and analyzed via a transmission line model. Finite element calculations confirm the considerations. The significance for impedance spectroscopy and solid-state ionics is discussed.

Introduction

The development of novel variants of impedance techniques is often accompanied by an extension of the commonly used frequency, resistance, and capacitance ranges. Novel techniques which enable localized probing of samples and, therefore, spatially resolving characterization, involve very high resistances and small capacitances.[1,2] In order to measure such high resistances and small capacitances, samples have to be shielded properly. In this manner, electrical noise and stray capacitances are significantly reduced, but, on the other hand, an additional problem appears; the dielectric coupling of the sample to the surrounding electrical shield, *i.e.*, the sample holder itself. In this paper it is shown that such capacitance between the sample and the shield may lead to considerable anomalies in the impedance spectra: the appearance of "inductive loops." The extent of such anomalies depends on the sample geometry and is especially pronounced in the case of using microelectrodes or probing thin films.

So-called inductive loops have often been measured in electrochemical experiments and are usually explained by complicated electrode kinetics.[3-5] However, the inductive loops addressed in this paper do not originate from the sample and/or electrode peculiarities but from the capacitive coupling between the sample and the sample holder. It is the purpose of this paper to explain the phenomenon and to develop a model which renders the evaluations of sample parameters from the impedance spectra (involving shielding capacitance effects) still possible.

Theoretical Consideration: The Sample-to-Shield Capacitance

The impedance of a sample is usually obtained in the way illustrated in Fig. 1a. The voltage U applied to the sample is measured from point 1 to ground while the current flowing through the sample is measured at point 2. The impedance $Z \equiv U_1/I_2$ calculated from the measured values of U_1 and I_2 corresponds to the true impedance of the sample only if there is no current sink or source between the points 1 and 2. Such sinks and sources appear if a displacement current flows between the sample and the shield (Fig. 1c). In this case the current measured at point 2 would be different from the current measured at point 1.

Figure 1b schematically shows the measurement principle of autobalance bridges such as HP 4284, HP 4192A, or Solartron 1260. The current measurement (via measuring U_2) is carried out at point 2 and thus takes no account of the current loss due to the displacement current between sample and shield. The situation may be at first approximated by the model explained in Fig. 1c; the sample is divided into two identical halves, each represented by a parallel RC term. The capacitive current to the shield is represented by the capacitor C_m. The real and the imaginary part of the effective impedance $Z \equiv Z_{re} + iZ_{im}$ corresponding to such an equivalent circuit as a function of the angular frequency ω read as

$$Z_{re} = \frac{R[1 + \omega^2 R^2 C(C + C_m)]}{(1 + \omega^2 R^2 C^2)^2} \quad [1a]$$

$$Z_{im} = -\frac{\omega R^2(\omega^2 R^2 C^2(2C + C_m) + 2C - C_m)}{(1 + \omega^2 R^2 C^2)^2} \quad [1b]$$

For a large enough shielding capacitance ($C_m > 2C$) the imaginary part of the effective impedance Z_{im} becomes positive for the frequencies

$$\omega < \sqrt{\frac{(C_m - 2C)}{(2C + C_m)R^2C^2}} \quad [2]$$

An impedance spectrum calculated according to Eq. 1a and 1b with $R = 10$ MΩ, $C = 1$ pF, and $C_m = 10$ pF is displayed in Fig. 2.

We term that part of the spectra, in which the imaginary part of the impedance is positive, the "inductive loop" (see Fig. 2). This inductive loop should not be confused with inductances of the wires which affect the impedance at high frequencies, especially in the case of well-conductive samples.

* Electrochemical Society Student Member.
[a] On leave from National Institute of Chemistry, SI-1001 Ljubljana, Slovenia.